São Paulo potential as a tool for calculating *S* factors of fusion reactions in dense stellar matter

L. R. Gasques,[1,*] A. V. Afanasjev,[1,2] M. Beard,[1] J. Lubian,[3] T. Neff,[4,†] M. Wiescher,[1] and D. G. Yakovlev[5]

[1]*Department of Physics & The Joint Institute for Nuclear Astrophysics, University of Notre Dame, Notre Dame, Indiana 46556, USA*

[2]*Department of Physics and Astronomy, Mississippi State University, P. O. Box 5167, Mississippi State, Mississippi 39762, USA*

[3]*Instituto de Física, Universidade Federal Fluminense, Av. Litorânea s/n, 24210-340 Niteroi, Riode Janeiro, Brazil*

[4]*NSCL, Michigan State University, East Lansing, Michigan 48824, USA*

[5]*Ioffe Physico-Technical Institute, Politekhnicheskaya 26, RU-194021 St. Petersburg, Russia*

(Received 3 January 2007; revised manuscript received 12 July 2007; published 24 October 2007)

The goal of this paper is to test and justify the use of the São Paulo potential model for calculating astrophysical *S* factors for reactions involving stable and neutron-rich nuclei. In particular, we focus on the theoretical description of *S* factors at low energies. This is important for evaluating the reaction rates in dense stellar matter. We calculate the *S* factors for a number of reactions (^{16}O+^{16}O, ^{20}O+^{20}O, ^{20}O+^{26}Ne, ^{20}O+^{32}Mg, ^{26}Ne+^{26}Ne, ^{26}Ne+^{32}Mg, ^{32}Mg+^{32}Mg, ^{22}O+^{22}O, ^{24}O+^{24}O) with the São Paulo potential in the framework of a one-dimensional barrier penetration model. This approach can be easily applied for many other reactions involving different isotopes. To test the consistency of the model predictions, we compare our calculations with those performed within the coupled-channels and fermionic molecular dynamics models. Calculated *S* factors are parametrized by a simple analytic formula. The main properties and uncertainties of reaction rates (appropriate to dense matter in cores of massive white dwarfs and crusts of accreting neutron stars) are outlined.

DOI: 10.1103/PhysRevC.76.045802 PACS number(s): 25.70.Jj, 21.30.Fe, 24.10.Ht, 26.50.+x

I. INTRODUCTION

In this paper, we investigate the model dependence of astrophysical *S* factors for fusion reactions involving stable and neutron-rich nuclei such as ^{16}O, ^{20}O, ^{22}O, ^{24}O, ^{26}Ne, and ^{32}Mg. With this approach, we seek to test the applicability of the São Paulo (SP) potential for computing *S* factors for a broad range of fusion reactions involving different isotopes.

As outlined in our previous work [1,2], the determination of the astrophysical *S* factor at low energies is needed for evaluating reaction rates in different stellar environments ranging from the core of massive stars during late stellar evolution to dense stellar matter of white dwarf cores and neutron star crusts. Of particular interest is the possibility of fusion induced burning in accreting neutron stars and white dwarfs. The accreted matter in the envelopes of neutron stars and in the interiors of white dwarfs is eventually compressed (and/or heated) under the weight of newly accreted material (and under the action of various energy release mechanisms) and undergoes nuclear transformations. These transformations involve β captures, fusion reactions, absorption, and emission of neutrons. β captures become especially important at densities $\rho \gtrsim 10^9$ g cm^{-3} (e.g., Ref. [3]). They lead to the appearance of neutron-rich isotopes which can further participate in nuclear fusion. At $\rho \sim (4\text{–}6) \times 10^{11}$ g cm^{-3}, neutrons begin to drip from neutron-rich atomic nuclei in the crust of neutron stars. As a result, the inner crust of a neutron star (the layer that extends from this neutron drip density to the neutron star core, to $\rho \sim 1.5 \times 10^{14}$ g cm^{-3}; see, e.g., Ref. [4]) consists of very neutron-rich atomic nuclei, electrons, and free neutrons.

Explosive burning of carbon and other elements in the cores of massive white dwarfs trigger type Ia supernova explosions (e.g., Ref. [5,6]). Thermonuclear burning of accreted matter in surface layers of neutron stars in compact binary systems produces type I x-ray bursts [7]. Deeper burning of carbon in accreting neutron stars is possibly responsible for superbursts observed from some x-ray bursters (e.g., Refs. [8–10]). Even deeper burning of accreted matter in pycnonuclear reactions and β captures in the crust of transiently accreting neutron stars [10–12] can power [13] thermal radiation observed from neutron stars in soft x-ray transients during quiescent states (see, e.g., Refs. [10,14,15]).

To study all these processes, one needs to know various nuclear transformation rates in huge ranges of density and temperature at drastically different physical conditions. For instance, nuclear reactions of hydrogen and helium burning in the surface layers of accreting neutron stars (producing type I x-ray bursts) occur in the thermonuclear regime (possibly with strong plasma screening [16]). In contrast, the reactions between very neutron-rich atomic nuclei in the inner neutron star crust [11,12] (e.g., ^{34}Ne+^{34}Ne $\rightarrow$ ^{68}Ca at $\rho \approx 1.5 \times 10^{12}$ g cm^{-3} [11]) are supposed to occur in the pycnonuclear regime, as a result of strong zero-point vibrations of atomic nuclei in Coulomb lattice (e.g., Ref. [17]). More details on various burning regimes can be found, for instance, in Refs. [1,2,18]. As a rule, one needs to consider multicomponent dense matter containing many isotopes. For instance, modern simulations of type I x-ray bursts involve up to 1300 isotopes [19]. The composition of burst ashes may depend on many parameters. The ashes burn further after sinking into deeper layers of the crust of an accreting neutron star [10]. Therefore, one should deal with many nuclear reactions.

*Present address: Department of Nuclear Physics, Research School of Physical Sciences and Engineering, Australian National University, Canberra, ACT 0200, Australia.

†New address: Gesellschaft für Schwerionenforschung mbH, Planckstr. 1, D-64291 Darmstadt, Germany.

The determination of fusion cross sections at extremely low energies remains a critical issue for calculating reaction rates of astrophysical interest. In the simplest framework, two heavy ions are assumed to fuse after tunneling through the Coulomb barrier. However, at subbarrier energies, large enhancements of the fusion cross section have been observed compared to theoretical predictions obtained with the barrier penetration (BP) model. At energies around and below the Coulomb barrier, couplings between fusion and other degrees of freedom become significant. Coupled-channels (CC) calculations have successfully explained the enhancements observed in the heavy-ion fusion subbarrier cross sections for a large number of reactions (e.g., Refs. [20,21]). Recently, hindrance of fusion cross sections occurring at extremely low energies for medium-mass systems has been suggested [22]. Even though this hindrance seems to depend on the entrance channel properties of the nuclei, its complete understanding has not yet been achieved. In particular, for reactions involving light nuclei such as ^{12}C and ^{16}O, it is not entirely clear whether the fusion cross sections at extreme subbarrier energies will be affected by this phenomenon. Future experiments at energies well below the Coulomb barrier are needed to clarify this point.

For reactions involving neutron-rich nuclei, which are expected to dominate pycnonuclear burning in the deep crust of accreting neutron stars [11,12,18], the situation gets even more complicated. The large spatial extent of the neutron matter may lower an average fusion barrier, resulting in an induced enhancement of fusion cross sections. Alternatively, the loosely bound halo nuclei can break up in the field of the other nucleus, leading to a loss of flux to peripheral reaction channels, thereby causing a hindrance of the fusion process [23–28]. Most of the calculations are qualitative, and a fully quantitative understanding of this process remains challenging. Because of the low intensity of radioactive beams, experimental investigation of reaction mechanisms with unstable beams is difficult. Studies with weakly bound stable nuclei currently allow more precise and extensive experimental measurements, but the results obtained so far have not been conclusive [29–38].

In earlier works [39,40], we adopted the BP formalism and the well-known parameter-free SP potential [41] in the analysis of fusion cross sections involving stable nuclei. The subbarrier data could be reasonably accounted for through the introduction of effective barrier parameters. However, the validity of the SP potential in providing a global description of fusion reactions for nuclei far from the stability valley has not been explored. Since no experimental data are available for fusion reactions between unstable nuclei, we compare the fusion cross sections obtained through the SP potential and the BP model with the results provided by a CC analysis performed with the FRESCO code [42]. In addition, we compare the BP results with predictions of the fermionic molecular dynamics (FMD) model [43]. Here, the nucleus-nucleus system is treated in the spirit of the microscopic cluster model [44,45]. The wave function is fully antisymmetrized and projected on angular momentum. The same effective nucleon-nucleon interaction [46] is used to determine the ground state and the nucleus-nucleus energy surface. The isospin degree of freedom is treated explicitly in the FMD model. The microscopic many-body nucleus-nucleus interaction is mapped in a two-step process [47] on a local nucleus-nucleus potential that takes into account the Pauli forbidden states. Solving the two-body Schrödinger equation with incoming wave boundary conditions (IWBC) [48,49], we obtain the fusion cross sections for the ^{16}O+^{16}O, ^{22}O+^{22}O, and ^{24}O+^{24}O reactions.

The goal of the present paper is to prove the reliability of the SP potential in predicting low-energy S factors for fusion reactions involving nuclei far from stability. The main point is to establish the uncertainties against more elaborated approaches such as the CC and FMD models. The advantage in adopting the SP potential and the BP model is that once the density distribution of the reacting nuclei is determined, no additional parameter is necessary to obtain the real part of the nuclear interaction. Furthermore, the CC and FMD calculations may be very time consuming. Hence, our simple phenomenological model gives us a powerful tool for predicting average low-energy S factors for many fusion reactions.

The paper is organized as follows. In Sec. II we outline the main points of the SP potential, BP model, and the CC analysis. In addition, we compare S factors for the ^{16}O+^{16}O, ^{20}O+^{20}O, ^{20}O+^{26}Ne, ^{20}O+^{32}Mg, ^{26}Ne+^{26}Ne, ^{26}Ne+^{32}Mg, and ^{32}Mg+^{32}Mg reactions obtained with and without taking coupling effects into account. Section III contains the description of the FMD calculations. The S factors computed using this formalism for the ^{16}O+^{16}O, ^{22}O+^{22}O, and ^{24}O+^{24}O reactions are compared with those provided by the BP model. We briefly discuss the properties of reaction rates in dense stellar matter in Sec. IV and conclude in Sec. V.

II. THE BARRIER PENETRATION MODEL

For calculating the fusion cross section using the BP model, we adopt the parameter-free nonlocal SP potential [41,50–52]. This potential has been used and tested in describing many reactions over a broad energy range [39–41,53–59]. The SP potential $V_{\rm SP}(R, E)$ is related to the folding potential $V_F(R)$ [60] through

$$V_{\rm SP}(R, E) = V_F(R)\ \exp(-4v^2/c^2), \tag{1}$$

where c is the speed of light, and v is the local relative velocity between the two nuclei,

$$v^2(R, E) = (2/\mu)\,[E - V_C(R) - V_{\rm SP}(R, E)], \tag{2}$$

where μ is the reduced mass, and $V_C(R)$ is the Coulomb potential. In the limit of $E \to 0$, Eq. (1) reduces to the usual expression for the folding potential. In particular, the Pauli nonlocality correction in the nuclear potential is negligible for the stellar nuclear reaction rates. However, the choice of the SP potential for calculating S factors remains valid since this phenomenological approach represents a general model that provides a better match to the energy dependence of the reaction cross sections. The folding potential depends on the matter densities of the reacting nuclei,

$$V_F(R) = \int \rho_1(\boldsymbol{r}_1)\rho_2(\boldsymbol{r}_2)V_0\delta(\boldsymbol{R} - \boldsymbol{r}_1 + \boldsymbol{r}_2)d^3r_1d^3r_2, \tag{3}$$

TABLE I. Inelastic channels included in the CC calculations. Excitation energies (in parentheses) are in MeV.

^{16}O	^{20}O	^{26}Ne	^{32}Mg
0^+(g.s.)	0^+(g.s.)	0^+(g.s.)	0^+(g.s.)
3^-(6.130)	2^+(1.673)	2^+(2.018)	2^+(0.885)
2^+(6.619)	4^+(3.570)		
	2^+(4.072)		
	0^+(4.456)		
	3^+(5.614)		

where $V_0 = -456$ MeV fm^3. The use of the matter densities and the δ function corresponds to the zero-range approach for the folding potential, which is equivalent [41] to the more usual procedure of adopting the M3Y effective nucleon-nucleon interaction with the nucleon densities of the nuclei. We adopt the relativistic Hartree-Bogoliubov (RHB) model to calculate the density distributions of the nuclei.

The calculation of the fusion cross section and the associated astrophysical factor $S(E)$ through the BP model requires the determination of the effective potential, defined as a sum of the Coulomb, nuclear, and centrifugal parts,

$$V_{\rm eff}(R, E) = V_C(R) + V_{\rm SP}(R, E) + \frac{\ell(\ell+1)\hbar^2}{2\mu R^2}. \quad (4)$$

The Coulomb potential has been calculated through a folding procedure using the charge densities obtained from the RHB model. In the BP model, the fusion cross section is associated to the flux transmitted through the barrier,

$$\sigma_{\rm BPM}(E) = \frac{\pi}{k^2} \sum_{\ell=0}^{\ell_{\rm max}} (2\ell+1)\, T_\ell. \quad (5)$$

The sum is performed up to a maximum $\ell = \ell_{\rm max}$, the largest angular momentum that produces a pocket in the effective potential (4).

Let us compare the S factors calculated using the SP potential and the BP model with those calculated by a CC method using the FRESCO code [42]. For CC calculations, it is important to determine the bare nuclear potential and the number of states or partitions to be included in the coupled reaction channel set. As in the BP model calculations, we have employed the SP potential as a bare potential in the CC analysis. As shown in Table I, we include only inelastic excitations to low-energy excited states (g.s. labels the ground states). The deformation length for the quadrupole and octupole excitations are taken from Refs. [61,62].

A. Density calculations in the relativistic Hartree-Bogoliubov theory

Deriving the cross sections for fusion reactions between light neutron-rich nuclei by using a folding nuclear potential model requires accurate modeling of the nuclear density distribution. There are several ways to determine these density distributions [63]. For example, density functional theories provide a successful description of many nuclear properties, in particular, of charge distributions in experimentally known nuclei. Because these models are universal in the sense that their parameters are carefully adjusted and valid all over the nuclear chart, one can expect that they also well describe nuclei far from stability. Nonrelativistic density functionals, such as the ones based on the Skyrme or Gogny forces [64], have been widely used in the literature.

In recent years, relativistic (covariant) density functionals have become very accurate in describing nuclear properties [65,66]. Best known is the RHB model [66–68], which includes pairing correlations with a finite-range pairing force. It provides a unified description of mean-field and pairing correlations in nuclei. These relativistic density functionals strongly depend on density, either through the nonlinear coupling terms between mesons and nucleons (e.g., in the Lagrangians with parameter sets NL3 [69]), or through explicit density dependence for meson-nucleon vertices (e.g., in the parameter set DD-ME2 [70]). Both parametrizations work well in neutron-rich nuclei [66,69,70] and accurately describe proton density distributions in the mass region of interest [1,66].

In the current work, the RHB densities are used. It is important to understand how the uncertainties in the calculations of the RHB densities affect the S factors obtained within the BP model. These uncertainties are due to the fact that particle-hole (mean field) and particle-particle (pairing) channels of the RHB model are not necessarily optimally parametrized. In addition, there are no experimental data on the tail of the density distribution at large distances from the nucleus center. Therefore, it is unknown how well modern theories describe the asymptotic tail of the density distribution. To resolve this issue, we study the dependence of calculated S factors on (i) the choice of the relativistic mean field (RMF) Lagrangian, (ii) the uncertainties related to the choice and treatment of pairing, and (iii) the uncertainties in the description of the tail of the density distribution.

For simplicity, we restrict ourselves to spherical nuclei. The RHB calculations were performed using the NL3 and DD-ME2 parametrizations of the RMF Lagrangian in the particle-hole channel and the central part of the D1S Gogny force [64] in the particle-particle channel. We take a number of C, O, Ne, and Mg isotopes from the β stability line to the neutron drip line.

The densities calculated with the NL3 and DD-ME2 parametrizations are similar. As a consequence, the difference in the S factors calculated in the BP formalism with respective RHB densities is rather small for the reactions involving nuclei close to the β stability line. However, the difference can reach a factor of 3 for the reactions involving neutron-rich nuclei, reflecting the fact that isospin properties of the RMF Lagrangians are not uniquely constrained.

To study the impact of pairing, the S factors of symmetric reactions involving O and Ne isotopes were calculated from the RHB densities with and without pairing. As shown in Fig. 1, the largest difference in the calculated density distributions is observed for the ^{22}O nucleus. The origin of this difference lies in the specifics of the shell structure of the neutron subsystem: the filling of the $\nu s_{1/2}$ subshell (as, for example, in the case in ^{24}O) considerably increases the density in the central part of the

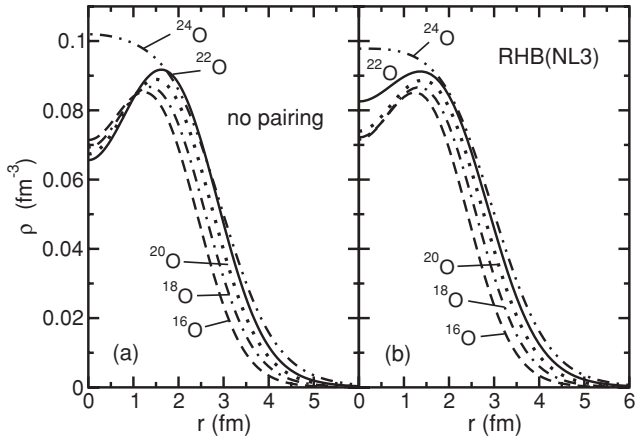

FIG. 1. Self-consistent RHB neutron densities for the ground states of oxygen isotopes obtained in the calculations (a) without and (b) with pairing.

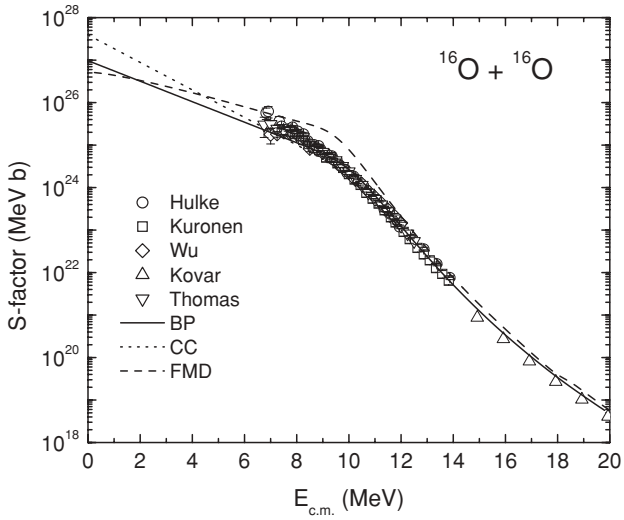

FIG. 2. ^{16}O+^{16}O astrophysical factors $S(E)$ as a function of the center-of-mass energy $E = E_{\mathrm{c.m.}}$. Lines show theoretical results obtained through the BP model (solid), CC calculations (dotted) and FMD (dashed) models. Various symbols present experimental results.

nucleus (Fig. 1). In ^{22}O, this subshell is empty in the absence of pairing, and it is partially filled when pairing is present. Consequently, the largest difference in $S(E)$ (of about a factor of 2) is observed for the ^{22}O+^{22}O reaction. For reactions involving neutron-rich Ne and Mg isotopes, only a marginal difference is observed in the results based on the different model parameters and treatment of pairing.

An additional uncertainty comes from the strength of the pairing force. Physical observables such as moments of inertia [68,71,72] and odd-even mass differences [72,73], which are sensitive to the pairing strength, are correctly described in many cases by the D1S Gogny force. However, there still are some cases where the modification of the strength of the D1S Gogny force by ≈10–15% is needed in order to reproduce experimental data [72]. Thus, the uncertainty in the strength of the pairing force can be estimated to be on the level of 15%. Such uncertainties do not appreciably modify the nuclear densities, and they affect $S(E)$ by a maximum factor of 2. In most cases, this factor is actually lower. The study of Ne isotopes also shows that either exact or approximate (by means of the Lipkin-Nogami method) particle number projection has little effect on densities and S factors.

Available experimental data on the proton density distributions cover the density range $\rho \approx 10^{-1}$–10^{-3} fm^{-3}. Thus, it is unclear how well existing theories describe the density profile at large distances from the nucleus center, where $\rho \lesssim 10^{-4}$ fm^{-3}. Different density profiles at radial distances corresponding to $\rho < 10^{-4}$ fm^{-3} were used to simulate the impact of the uncertainties in the asymptotic tail of density distribution on $S(E)$. It turns out that even a drastic (definitely unphysical) assumption that $\rho \to 0$ as soon as $\rho = 10^{-4}$ fm^{-3} changes $S(E)$ very little (by a factor $\lesssim$2 only at some reaction energies). Thus, possible uncertainties in the calculated asymptotic tail of the density distribution at $\rho \lesssim 10^{-4}$ fm^{-3} are unimportant.

In summary, the uncertainties in $S(E)$ (and corresponding reaction rates) due to nuclear structure effects are expected to be smaller than one order of magnitude even if the reactions involve neutron-rich nuclei. For many astrophysical reactions, such a description is satisfactory, since the uncertainties related to the plasma physics can reach many orders of magnitude (Sec. IV).

B. *S* factor results with and without coupling effects

In Fig. 2, we compare the BP model and CC calculations against the measured [74–78] ^{16}O+^{16}O fusion S factors. The S factors obtained with the BP model were previously shown in Fig. 1 of Ref. [2]. We present these results again to compare our simple phenomenological approach against more sophisticated theoretical models such as CC and FMD. The agreement between data and theoretical predictions obtained with a single- and coupled-channels analyses (solid and dotted lines, respectively) is satisfactory considering that there are no free parameters included in the calculations. At extremely low energies, where no experimental data are available, the difference between the CC and BP results does not exceed a factor of 4. At such low energies, we might expect a negligible effect of couplings. However, for the determination of astrophysical reaction rates, the calculated S factor must be extrapolated toward the energy region of astrophysical interest. Therefore, the determination of S factors at extremely low energies is not completely independent of the S factors calculated at energies around the Coulomb barrier. In this way, couplings might affect the determination of low-energy $S(E)$. For astrophysical applications, a discrepancy of a factor of 4 between the theoretical calculations can be disregarded (Sec. IV). In calculating the SP potential, two colliding spherical nuclei are considered in the simple approach of frozen densities. Hence, a treatment including resonant effects is beyond the scope of this work. In particular, resonances in the fusion excitation function for the ^{16}O+^{16}O reaction are much less pronounced than those observed for the ^{12}C+^{12}C and ^{12}C+^{16}O reactions. This gives us confidence in the

TABLE II. The coefficients $A_1, \ldots, A_5$ and E_0 in the fits expression (6) for all calculated S factors.

Reaction	Model	E_0	A_1	A_2	A_3	A_4	A_5
^{16}O+^{16}O	BP	10.52	56.16	−0.571	−1.160	−1.044	0.0366
^{16}O+^{16}O	CC	10.73	55.47	−0.754	−1.05	−0.749	0.0276
^{16}O+^{16}O	FMD	10.14	58.11	−0.358	−2.00	−1.315	0.0365
^{20}O+^{20}O	BP	10.65	64.24	−0.737	−3.41	−0.941	0.0325
^{20}O+^{20}O	CC	10.15	64.77	−0.738	−2.49	−1.117	0.0400
^{20}O+^{26}Ne	BP	12.42	77.97	−0.742	−3.03	−1.059	0.0200
^{20}O+^{26}Ne	CC	12.20	78.41	−0.885	−2.83	−0.949	0.0130
^{20}O+^{32}Mg	BP	14.35	90.28	−0.755	−2.72	−1.197	0.0260
^{20}O+^{32}Mg	CC	13.99	90.98	−0.951	−2.59	−0.965	0.0090
^{26}Ne+^{26}Ne	BP	14.88	95.03	−0.756	−3.03	−1.203	0.0210
^{26}Ne+^{26}Ne	CC	14.61	96.82	−0.732	−5.19	−0.627	−0.0720
^{26}Ne+^{32}Mg	BP	17.16	110.75	−0.770	−2.42	−1.410	0.0316
^{26}Ne+^{32}Mg	CC	16.52	112.30	−0.953	−2.31	−1.331	0.0342
^{32}Mg+^{32}Mg	BP	20.32	129.51	−0.770	−3.62	−1.203	0.0041
^{32}Mg+^{32}Mg	CC	18.79	133.43	−0.757	−3.86	−1.216	−0.0118
^{22}O+^{22}O	BP	9.90	69.28	−0.832	−3.17	−1.200	0.0453
^{22}O+^{22}O	FMD	9.19	71.85	−0.487	−3.07	−1.832	0.0568
^{24}O+^{24}O	BP	9.51	74.44	−0.916	−4.20	−1.304	0.0498
^{24}O+^{24}O	FMD	8.47	78.75	−0.129	−4.49	−2.564	0.0676

extrapolation of the ^{16}O+^{16}O S factor toward low energies. As reported in Ref. [2], the BP model can be adopted to calculate the S factor for the ^{16}O+^{16}O reaction over the entire energy range.

For convenience of applications, we parametrize all calculated S factors by the equation [2]

$$S(E) = \exp\left(A_1 + A_2\,\Delta E + \frac{A_3 + A_4\,\Delta E + A_5\,\Delta E^2}{1 + \exp(-\Delta E)}\right) \text{ MeV b}, \qquad (6)$$

where $\Delta E = E - E_0$; the center-of-mass energy E and the fit parameter E_0 are expressed in MeV. The parameter E_0 is approximately equal to the height of the Coulomb barrier. The fit expression reflects different behavior of $S(E)$ above and below the barrier. The fit parameters are presented in Table II. The fits cover the energy ranges $E \leqslant E_{\max}$, where $E_{\max} =$ 18 MeV for C+C and O+O reactions; 20 MeV for C+Ne, O+Ne, Ne+Ne, C+Mg, and O+Mg reactions; and 22 MeV for Ne+Mg and Mg+Mg reactions. In most cases, formal maximum fit errors do not exceed 10–30%, being smaller than expected intrinsic errors of selected theoretical models. This fitting accuracy is more than sufficient for astrophysical applications.

In Fig. 3, we compare the BP (solid lines) and CC (closed circles) calculations for the reactions ^{20}O+^{20}O, ^{20}O+^{26}Ne, ^{20}O+^{32}Mg, ^{26}Ne+^{26}Ne, ^{26}Ne+^{32}Mg, and ^{32}Mg+^{32}Mg. Couplings hardly affect $S(E)$ at energies above the barrier but mainly enhance $S(E)$ at the subbarrier energies. Despite the somewhat large discrepancies between the two approaches at extremely low energies, the SP potential in the basis of the BP model still can be employed in the determination of the astrophysical S factor (see Sec. IV). In particular, the CC S factors for the ^{26}Ne+^{32}Mg reaction are about two orders of magnitude larger than those obtained with a single-channel potential at very small energies. Discrepancies between the BP and CC calculations are smaller for all other reactions studied in this paper.

For the ^{20}O+^{20}O case, the one- and two-neutron transfers to the lower excited state channels were included in the coupling scheme in order to verify its influence on $S(E)$. These couplings turn out to be negligible at energies below and above the Coulomb barrier.

III. THE FERMIONIC MOLECULAR DYNAMICS MODEL

The FMD model uses a completely different theoretical approach to determine the fusion cross sections of reactions involving both stable and neutron-rich nuclei. In this context, such calculations provide an independent test for the reliability of the SP potential and the BP model. In this section, we present S factors for the ^{16}O+^{16}O, ^{22}O+^{22}O, and ^{24}O+^{24}O reactions calculated at energies above and well below the Coulomb barrier. Technical details are provided in a separate publication [79].

In the FMD model [43,46], Slater determinants built out of Gaussian wave packets are used as many-body basis states. The mean positions, mean momenta, and widths of the wave packets as well as the orientation of spins are treated as variational parameters. The isospin of each wave packet is fixed to represent either a proton or a neutron.

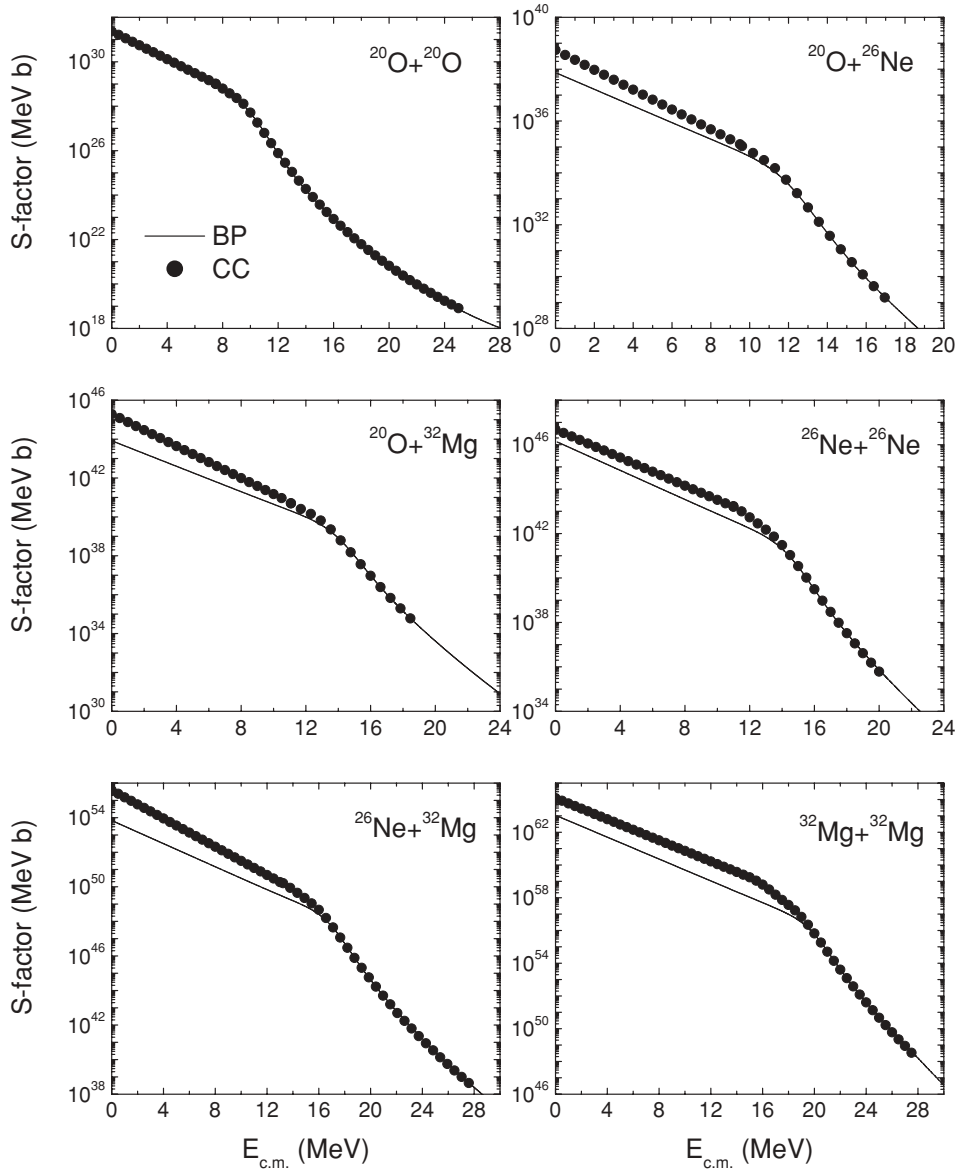

FIG. 3. Astrophysical factor $S(E)$ as a function of the center-of-mass energy $E = E_{\text{c.m.}}$ for the ^{20}O+^{20}O, ^{20}O+^{26}Ne, ^{20}O+^{32}Mg, ^{26}Ne+^{26}Ne, ^{26}Ne+^{32}Mg, and ^{32}Mg+^{32}Mg reactions. The solid lines are obtained with the SP potential and the BP model, whereas the closed circles correspond to the CC analysis. See text for details.

An effective interaction based on the realistic Argonne V18 interaction is used. The essential short-range central and tensor correlations are treated explicitly using the unitary correlation operator method (UCOM) [80,81]. A phenomenological modification of the correlated interaction that simulates effects of missing three-body correlations and genuine three-body forces is added and adjusted to reproduce experimental binding energies and radii for doubly magic nuclei. This interaction has been successfully used to describe binding energies and radii of nuclei in the p and sd shells [46].

To obtain the ground state wave functions, the expectation value of the intrinsic energy is minimized with respect to the parameters of the single-particle states. For the oxygen isotopes considered here, the ground states are found to be spherical and identical to closed-shell harmonic oscillator configurations.

The Gaussian basis allows one to easily translate and rotate the wave functions and can therefore be used to build many-body states for the nucleus-nucleus system in the spirit of a microscopic cluster model [44],

$$|\Psi(\boldsymbol{R})\rangle = \mathcal{A}\{|\psi(-\boldsymbol{R}/2)\rangle \otimes |\psi(\boldsymbol{R}/2)\rangle\}\,. \tag{7}$$

The states of the individual clusters are given by the Slater determinants $|\psi\rangle$. The antisymmetrization operator $\mathcal{A}$ exchanges nucleons between the clusters. The mean separation $\boldsymbol{R}$ between the clusters plays the role of the generator coordinate in the language of the generator coordinate method (GCM). To restore the rotational symmetry of the Hamiltonian, the basis states have to be projected on angular momentum [45,82]. For the sake of simplicity, we will nevertheless use the unprojected states in the following discussion.

The Slater determinants [Eq. (7)] provide a convenient basis for the evaluation of matrix elements, but they cannot be directly mapped onto a two-body picture with pointlike nuclei. Such a mapping can be achieved using a procedure proposed by Friedrich [47]. In the GCM basis states, the relative motion of the two nuclei is entangled with the intrinsic motion of the two nuclei and the total center-of-mass motion. In this respect,

the resonating group method (RGM) basis states $|\Phi(\boldsymbol{r})\rangle$ [45]

$$\langle \boldsymbol{\rho}, \xi_1, \xi_2 | \Phi(\boldsymbol{r})\rangle = \mathcal{A}\{\delta(\boldsymbol{r}-\boldsymbol{\rho})\phi(\xi_1)\phi(\xi_2)\} \tag{8}$$

are more convenient. Here, the intrinsic wave functions for the nuclei are given by $\phi(\xi_1)$ and $\phi(\xi_2)$, while $\boldsymbol{r}$ represents the cluster separation. If the intrinsic degrees of freedom are frozen, the RGM wave function depends solely on $\boldsymbol{r}$, and we can write the GCM basis states as

$$|\Psi(\boldsymbol{R})\rangle = \int d^3r\, \Gamma(\boldsymbol{R}, \boldsymbol{r})|\Phi(\boldsymbol{r})\rangle \otimes |\Phi_{\text{c.m.}}\rangle. \tag{9}$$

The function

$$\Gamma(\boldsymbol{R}, \boldsymbol{r}) = \left(\frac{\mu_A}{\pi a}\right)^{3/4} \exp\left(-\mu_A \frac{(\boldsymbol{R}-\boldsymbol{r})^2}{2a}\right),$$
$$\mu_A = \frac{A_1 A_2}{A_1 + A_2}, \tag{10}$$

(a is the width parameter of the wave packets) describes the relative motion of the nuclei within the Slater determinant. The center-of-mass motion, given by $|\Phi_{\text{c.m.}}\rangle$, decouples completely from the internal degrees of freedom.

Whereas the RGM basis states are already asymptotically orthogonal, that is,

$$\langle \Phi(\boldsymbol{r})|\Phi(\boldsymbol{r}')\rangle \overset{r,r'\to\infty}{\propto} \delta(\boldsymbol{r}-\boldsymbol{r}'), \tag{11}$$

the antisymmetrization destroys the orthogonality at short distances, where the two nuclei overlap. We therefore define new basis states

$$|\tilde{\Phi}(\boldsymbol{r})\rangle = \int d^3r' |\Phi(\boldsymbol{r}')\rangle n^{-1/2}(\boldsymbol{r}', \boldsymbol{r}), \tag{12}$$

using the RGM norm kernel

$$n(\boldsymbol{r}, \boldsymbol{r}') = \langle \Phi(\boldsymbol{r})|\Phi(\boldsymbol{r}')\rangle. \tag{13}$$

These new basis states are now orthonormal and can finally be used to map the microscopic description with Slater determinants [Eq. (7)] onto a collective picture using pointlike nuclei. Technically, the transformation in Eq. (12) requires the diagonalization of the RGM norm kernel, which is performed numerically. Eigenstates of the norm kernel with zero eigenvalues correspond to Pauli forbidden states.

The basis states [Eq. (12)] could be used to directly define a (necessarily nonlocal) nucleus-nucleus potential. For simplicity and to provide some physical insight, we instead follow Friedrich [47] and fit a local equivalent potential $V_N(r)$ to the GCM matrix elements of the intrinsic Hamiltonian (where the kinetic energy of the center-of-mass motion $T_{\text{c.m.}}$ has been subtracted),

$$\langle \Psi(\boldsymbol{R})|H - T_{\text{c.m.}}|\Psi(\boldsymbol{R})\rangle$$
$$\overset{!}{=} \int d^3r\, \tilde{\Gamma}(\boldsymbol{R}, \boldsymbol{r}) \left(-\frac{\hbar^2}{2\mu}\nabla^2 + V_C(r) + V_N(r) + E_1 + E_2\right) \tilde{\Gamma}(\boldsymbol{R}, \boldsymbol{r}). \tag{14}$$

The use of

$$\tilde{\Gamma}(\boldsymbol{R}, \boldsymbol{r}) = \int d^3r'\, n^{1/2}(\boldsymbol{r}, \boldsymbol{r}')\Gamma(\boldsymbol{R}, \boldsymbol{r}') \tag{15}$$

reflects the effects of antisymmetrization between the two clusters. The Coulomb potential $V_C(r)$ is that of two homogeneously charged spheres; E_1 and E_2 are the intrinsic energies of the nuclei. The fit is performed for the $\ell = 0, 2, 4$ partial waves. As the resulting potentials are almost identical, we make a combined fit for the different partial waves and obtain a single effective nucleus-nucleus potential $V_N(r)$.

This potential is finally used to solve the Schrödinger equation with incoming wave boundary conditions [48,49]. We assume here that the two nuclei will fuse if they reach the minimum in the potential surface behind the Coulomb barrier. The solution outside the range of the nucleus-nucleus potential is matched to the Coulomb wave functions to obtain the penetration probabilities for all possible partial waves.

These calculations are obtained using only frozen configurations and correspond to single-channel calculations of the fusion cross sections. To estimate the coupling to other channels, we create FMD configurations for the combined system of the two nuclei with constraints on the quadrupole deformation. When compared with the frozen configurations [Eq. (7)], we see almost no change for the GCM nucleus-nucleus energy surface in the barrier region. For smaller separations, the system tries to avoid the repulsion caused by antisymmetrization and deforms, thereby lowering the energy. As the energy surface in the region of the barrier is almost unchanged, we expect the effect of other channels on the fusion cross sections to be small.

As indicated by the dashed line in Fig. 2, the FMD calculations for the ^{16}O+^{16}O reaction present a slightly worse agreement with the data at energies around the Coulomb barrier ($V_B \sim 10.2$ MeV). The discrepancy between the results obtained via the FMD and BP models is not larger than a factor of 4 over the entire range of energy. In the limit of $E \to 0$, the difference between the two calculations is roughly a factor of 2. For the reactions involving neutron-rich nuclei, such as ^{22}O+^{22}O and ^{24}O+^{24}O, the FMD S factors are presented as open circles in Fig. 4. The comparison to the BP model results (solid lines) indicates a good agreement between the two theoretical models at energies above the Coulomb barrier. At subbarrier energies, the S factor for the ^{22}O+^{22}O reaction obtained from the FMD model is in reasonable agreement with predictions of the BP model. At extremely low energies, the difference between the theoretical calculations is approximately a factor of 5. For the ^{24}O+^{24}O reaction, the situation is somewhat worse, and the discrepancies between the two predictions reach up to two orders of magnitude in the limit of small energies. The FMD model predicts an almost constant S factor for the ^{24}O+^{24}O reaction at subbarrier energies, whereas the S factors calculated via the BP model follow an exponential behavior.

IV. REACTION RATES

In the following, we outline the impact of calculated S factors on fusion reaction rates in dense stellar matter. We do not consider a realistic composition of stellar matter since that would require more detailed reaction network simulations, but we discuss two fiducial examples of pure ^{16}O and pure ^{22}O

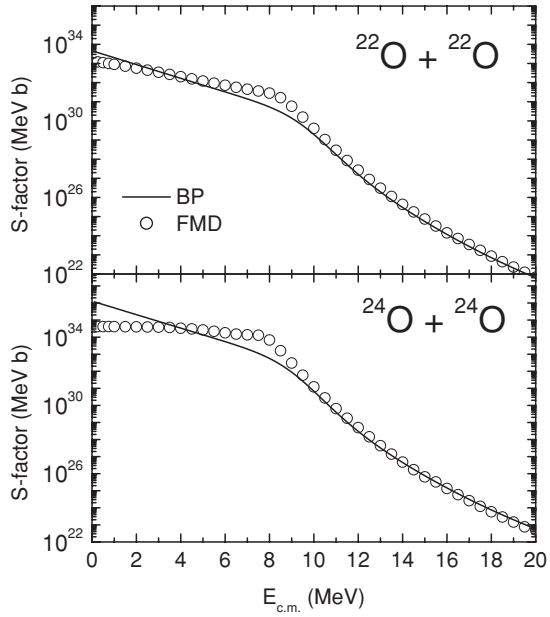

FIG. 4. Astrophysical factors $S(E)$ as a function of the center-of-mass energy $E = E_{\text{c.m.}}$ for the ^{22}O+^{22}O and ^{24}O+^{24}O reactions, derived from the SP potential and BP model (solid lines) and from the FMD calculations (open circles).

matter at a density $\rho = 5 \times 10^9$ g cm^{-3} typical for cores of massive white dwarfs and outer crusts of neutron stars. The ^{16}O isotope is stable in the laboratory and remains stable against β captures at the given density. The ^{22}O isotope is very neutron rich and thus unstable in the laboratory, but it becomes stable against β decays in our scenario because relativistic degenerate electrons in the stellar matter block β decays. At the chosen density, the electrons are still insufficiently energetic to initiate β captures on ^{22}O, so our illustrative ^{22}O matter is, in principle, stable.

Figure 5 shows the temperature dependence of the ^{16}O+^{16}O reaction rate in pure ^{16}O matter (left panel) and of the ^{22}O+^{22}O reaction rate in pure ^{22}O matter (right panel). In the displayed temperature range, plasma ions (oxygen nuclei) form a strongly coupled Coulomb plasma. At temperatures $T \gtrsim 5 \times 10^7$ K, it is liquid; while at lower T, it solidifies. The ion plasma temperature, which measures the importance of quantum effects in ion motion, is $T_p \sim 2 \times 10^8$ K. Recall that the reaction rates are determined by plasma physics effects (Coulomb barrier penetration in dense plasma environment) and nuclear physics effects (S factors). At sufficiently high temperatures, $T \gtrsim T_p$, oxygen burning at conditions displayed in Fig. 5 proceeds in the thermonuclear regime (owing to the thermal energy of reacting nuclei) with strong plasma screening. The reaction rates exponentially decrease with decreasing temperature, although the plasma screening effects greatly enhance the rates. The Gamow peak energy of the most efficiently reacting nuclei decreases and drops below the range accessible in laboratory experiments. At $T \lesssim T_p$ the nuclei burn in the pycnonuclear regime owing to zero-point vibrations in the strongly coupled plasma. In this case, the reaction rates weakly depend on the temperature but exponentially depend on the density (e.g., Ref. [17]). At $T \lesssim 5 \times 10^7$ K, for the given density, the rates become temperature independent. The energy of the reacting nuclei becomes $\sim k_B T_p$ [17], where k_B is the Boltzmann constant. Because the ^{22}O nuclei are more massive than ^{16}O, their zero-point vibrations are weaker and the pycnonuclear reaction rates are much lower, as seen by comparing the left and right panels of Fig. 5.

As a first step, let us adopt the optimal Coulomb tunneling model of Ref. [1] and the S factors obtained with the SP potential. In Fig. 5, the corresponding reaction rates are plotted by thick solid lines. The hatched regions show current theoretical uncertainties of the Coulomb tunneling problem for these S factors. They are limited by the maximum and minimum Coulomb tunneling penetrability from Ref. [1]. We see that in the thermonuclear burning regime, the plasma physics uncertainties are reasonably small, but in the pycnonuclear regime, they reach approximately 10 orders of magnitude. They are much larger than the maximum uncertainties of about two orders of magnitude in the low-energy S factors deduced from different calculations for some reactions (Secs. II B and III). The nature of the plasma physics uncertainties is summarized in Ref. [1]. They are mainly due to unknown microstructure of cold Coulomb plasma in stellar matter (a body-centered cubic or face-centered cubic crystal, a disordered state, a crystal with defects, etc.). They partly come from the not fully explored response of neighboring ions to the Coulomb tunneling of

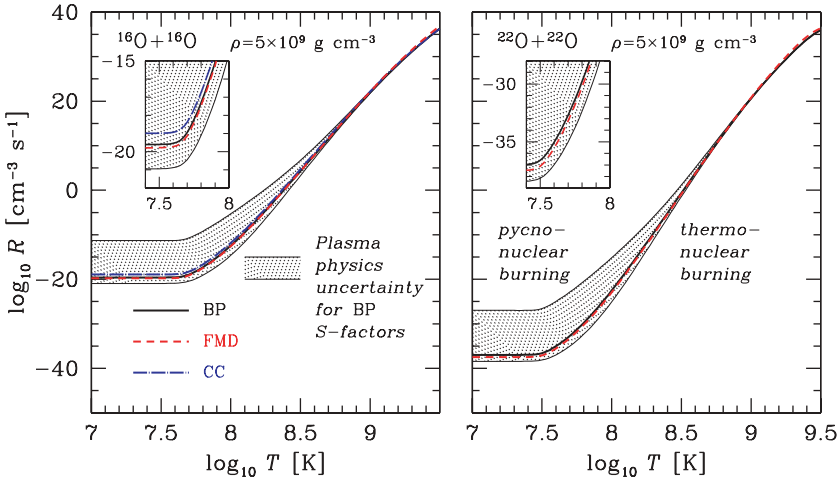

FIG. 5. (Color online) Temperature dependence of the ^{16}O+^{16}O reaction rate R in ^{16}O matter (left) and of the ^{22}O+^{22}O reaction rate in ^{22}O matter (right) at a density $\rho = 5 \times 10^9$ g cm^{-3}. The solid, dashed, and dot-dashed lines are calculated, respectively, with the BP, FMD, and CC S factors using the optimal Coulomb tunneling model [1]. Hatched regions show current theoretical uncertainties of Coulomb tunneling models [1] employing the BP S factors. Insets display some fragments on a larger scale. See text for details.

the reacting nuclei (static or fully relaxed crystalline lattice models of Ref. [17], or intermediate dynamical response) and from other delicate features of Coulomb tunneling in dense stellar matter.

By way of comparison, let us adopt the optimal Coulomb tunneling model and use different nuclear physics input (different S factors, keeping in mind that the reaction rates are directly proportional to S). The dashed lines in both panels of Fig. 5 are calculated using the FMD S factors, while the dot-dashed line in the left panel is obtained with the CC S factor. We see that the uncertainties of the reaction rates introduced by the different theoretical S factor models are much smaller than those introduced by plasma screening effects. The thick solid, dashed, and dot-dashed curves are almost indistinguishable in the main panels of Fig. 5, but they can be distinguished in the inserts. The uncertainties are of the same order of magnitude for the reactions involving stable isotopes and very neutron-rich isotopes. Therefore, one can definitely use the SP potential in the basis of the BP model for calculating the S factors to be employed as a physics input to compute numerous reaction rates of astrophysical importance. It is the plasma physics problem in the pycnonuclear regime which prevents calculation of accurate reaction rates in a rather cold stellar matter.

Let us remark that the largest uncertainties of about two orders of magnitude between the S factors calculated by the BP and CC methods for the ^{26}Ne+^{32}Mg reaction (see Sec. II B) and by the BP and FMD methods for the ^{24}O+^{24}O reaction (see Sec. III) occur at the lowest collision energies. Therefore, they introduce the largest uncertainties into the reaction rates only in the pycnonuclear regime where much larger plasma physics uncertainties are expected.

Finally, let us emphasize that even sufficiently large uncertainties in $S(E)$ are not very important for astrophysical applications. This is because the reaction rates are very rapidly varying functions of the temperature (in the thermonuclear regime, $T \gtrsim T_p$) or the density (in the pycnonuclear regime, $T \lesssim T_p$). Therefore, even large deviations of the reaction rate due to the uncertainties in $S(E)$ can be easily absorbed by small shifts of T (at $T \gtrsim T_p$) or ρ (at $T \lesssim T_p$). For instance, let us consider pure ^{16}O matter at $\rho = 5 \times 10^9$ g cm^{-3} and $T = 10^9$ K, corresponding to the thermonuclear burning regime in the left panel of Fig. 5, and adopt the SP potential in the basis of the BP model. In this case, the ^{16}O+^{16}O reaction rate is $R \approx 8.8 \times 10^{21}$ cm^{-3} s^{-1}. If we artificially increase $S(E)$ by one order of magnitude, the reaction rate at $T = 10^9$ K will increase by the same factor, but we can easily restore the initial rate by dropping the temperature to 9.3×10^8 K ($\sim$7%). Such temperature shifts are often insignificant.

For instance, consider a temperature profile $T(\rho)$ in the outer envelope of a steadily accreting neutron star in the regime of stable nuclear burning of accreted matter (see, e.g., Ref. [10] and references therein). This profile is determined by the balance of the nuclear energy generation rate and the thermal energy outflow (mainly by thermal conduction to the stellar surface). The thermal conduction outflow is a slowly varying function of temperature which cannot be affected by 10% temperature variations. Therefore, in a hot ^{16}O matter at $\rho \sim 5 \times 10^9$ g cm^{-3} in our illustrative example, a factor of 10 uncertainty in $S(E)$ will translate into $\sim$7% lowering of the temperature profile $T(\rho)$ which will hardly affect observational properties of the neutron star. We can add that the nuclear physics uncertainties of $S(E)$ will also be smoothed in a multicomponent matter with many nuclear reaction chains.

V. CONCLUSIONS

The astrophysical S factors are a necessary component for calculating fusion reaction rates in dense stellar matter of white dwarf cores and neutron star envelopes. To this aim, one needs S factors at low energies which cannot be measured in laboratory experiments and can only be computed.

We have calculated S factors for a number of fusion reactions (^{16}O+^{16}O, ^{20}O+^{20}O, ^{20}O+^{26}Ne, ^{20}O+^{32}Mg, ^{26}Ne+^{26}Ne, ^{26}Ne+^{32}Mg, ^{32}Mg+^{32}Mg, ^{22}O+^{22}O, ^{24}O+^{24}O) using the SP potential and the BP model. The reactions involve stable and neutron-rich nuclei. We have compared these S factors with those determined by CC and FMD calculations, which require much larger computer resources. Our main conclusions are the following:

(i) The overall agreement between the S factors calculated by the BP, CC, and FMD methods is satisfactory for calculating the fusion reaction rates involving nuclei far off stability at the extreme temperature and/or density conditions of astrophysical importance.

(ii) The largest difference of calculated S factors reaches two orders of magnitude at the lowest collision energies for the ^{26}Ne+^{32}Mg and ^{24}O+^{24}O reactions, comparing the BP results with the CC and FMD calculations, respectively. Such a difference translates into uncertainties of the corresponding reaction rates in stellar matter, which reach a maximum of two orders of magnitude in the pycnonuclear regime. However, much larger uncertainties into the pycnonuclear rates come from the plasma physics problem which entails the calculation of the tunneling probability taking into account the influence of the Coulomb interaction between the reacting nuclei by plasma particles. It is the plasma physics problem in the pycnonuclear regime which should be accurately solved first of all.

(iii) Considering the simplicity of the SP potential and the BP model, and the absence of free adjustable parameters in these calculations, we conclude that it is the best tool for computing the S factors for numerous reactions of astrophysical interest that involve stable and neutron-rich isotopes.

(iv) All the S factors computed here by different methods are parametrized by simple analytic expressions to facilitate their applications in computer codes. Many other S factors, which can be calculated using the BP model, can be parametrized in the same way to produce a bank of uniform S factor data.

Finally, it should be mentioned that the procedure of extrapolating S factors discussed above does not include the possibility of a low-energy hindrance of fusion reactions

as suggested in Ref. [22]. Recently, Jiang *et al*. [83] have proposed a phenomenological extrapolation of the low-energy S factor which would cause a dramatic decline of S factor toward lower energies and consequently significantly reduce the reaction rate to an extent that pycnonuclear burning would be extremely slow. These results are speculative and disagree with the low-energy predictions of the FMD approach which inherently should have reflected such a hindrance term [79]. We will nevertheless discuss the consequences and implications of such low-energy fusion behavior in a forthcoming paper.

We are now at a stage to include a unified description of pycnothermonuclear reaction rates [2] in a network code to simulate nucleosynthesis in high-density stellar matter. We expect that our results will be useful to the study of nuclear reactions in the cores of accreting white dwarfs and in the envelopes of accreting neutron stars and to the simulation of a number of important astrophysical phenomena, for instance, x-ray bursts and superbursts, and deep crustal heating in accreting neutron stars.

ACKNOWLEDGMENTS

This work was partially supported by the Joint Institute for Nuclear Astrophysics (JINA) NSF PHY 0216783, the U.S. Department of Energy Grant DE-FG02-07ER41459, the Russian Foundation for Basic Research (Grants 05-02-16245 and 05-02-22003), and the Russian Federal Agency for Science and Innovations (Grant NSh 9879.2006.2).

[1] L. R. Gasques, A. V. Afanasjev, E. F. Aguilera, M. Beard, L. C. Chamon, P. Ring, M. Wiescher, and D. G. Yakovlev, Phys. Rev. C **72**, 025806 (2005).
[2] D. G. Yakovlev, L. R. Gasques, M. Beard, M. Wiescher, and A. V. Afanasjev, Phys. Rev. C **74**, 035803 (2006).
[3] S. L. Shapiro and S. A. Teukolsky, *Black Holes, White Dwarfs, and Neutron Stars* (Wiley-Interscience, New York, 1983).
[4] P. Haensel, A. Y. Potekhin, and D. G. Yakovlev, *Neutron Stars. 1. Equation of State and Structure* (Springer, New York, 2007).
[5] J. C. Niemeyer and S. E. Woosley, Astrophys. J. **475**, 740 (1997).
[6] P. Höflich, Nucl. Phys. **A777**, 579 (2006).
[7] T. Strohmeyer and L. Bildsten, in *Compact Stellar X-Ray Sources*, edited by W. H. G. Lewin and M. Van der Klis (Cambridge University, Cambridge, England, 2006), p. 113.
[8] H. Schatz, L. Bildsten, and A. Cumming, Astrophys. J. **583**, L87 (2003).
[9] A. Cumming, J. Macbeth, J. J. M. in't Zand, and D. Page, Astrophys. J. **646**, 429 (2006).
[10] S. Gupta, E. F. Brown, H. Schatz, P. Moeller, and K.-L. Kratz, Astrophys. J. **662**, 1188 (2007).
[11] P. Haensel and J. L. Zdunik, Astron. Astrophys. **229**, 117 (1990).
[12] P. Haensel and J. L. Zdunik, Astron. Astrophys. **404**, L33 (2003).
[13] E. F. Brown and L. Bildsten, Astrophys. J. **496**, 915 (1998).
[14] D. Page, U. Geppert, and F. Weber, Nucl. Phys. **A777**, 497 (2006).
[15] K. P. Levenfish and P. Haensel, Astrophys. Space Sci. **308**, 457 (2007).
[16] E. E. Salpeter, Aust. J. Phys. **7**, 373 (1954).
[17] E. E. Salpeter and H. M. Van Horn, Astrophys. J. **155**, 183 (1969).
[18] M. Beard and M. Wiescher, Rev. Mex. Fis. **49**, supl. 4, 139 (2003).
[19] S. E. Woosley, A. Heger, A. Cumming, R. D. Hoffman, J. Pruet, T. Rauscher, J. L. Fisker, H. Schatz, B. A. Brown, and M. Wiescher, Astrophys. J. Suppl. Ser. **151**, 74 (2004).
[20] A. M. Stefanini *et al*., in *Proceedings of the Workshop on Heavy Ion Fusion, Exploring the Variety of Nuclear Properties, Padova, Italy, 1994* (World Scientific, Singapore, 1994).
[21] M. E. Brandan and G. R. Satchler, Phys. Rep. **285**, 143 (1997).
[22] C. L. Jiang, B. B. Back, H. Esbensen, R. V. F. Janssens, and K. E. Rehm, Phys. Rev. C **73**, 014613 (2006).
[23] M. S. Hussein, M. P. Pato, L. F. Canto, and R. Donangelo, Phys. Rev. C **46**, 377 (1992).
[24] M. C. S. Figueira, E. M. Szanto, A. Szanto de Toledo, M. P. Pato, M. S. Hussein, and L. F. Canto, Phys. Rev. C **46**, 1139 (1992).
[25] C. H. Dasso and A. Vitturi, Phys. Rev. C **50**, R12 (1994).
[26] L. F. Canto, R. Donangelo, P. Lotti, and M. S. Hussein, Phys. Rev. C **52**, R2848 (1995).
[27] L. F. Canto, R. Donangelo, Lia M. de Matos, M. S. Hussein, and P. Lotti, Phys. Rev. C **58**, 1107 (1998).
[28] K. Hagino, A. Vitturi, C. H. Dasso, and S. M. Lenzi, Phys. Rev. C **61**, 037602 (2000).
[29] A. Youshida, C. Signorini, T. Fukuda, Y. Watanabe, N. Aoi, M. Hirai, M. Ishihara, H. Kobinata, Y. Mizoi, L. Mueller, Y. Nagashima, J. Nakano, T. Nomura, H. Pu Y., and F. Scarlassara, Phys. Lett. **B389**, 457 (1996).
[30] P. A. De Young, B. Hughey, P. L. Jolivette, G. F. Peaslee, J. J. Kolata, V. Guimarães, D. Peterson, P. Santi, H. C. Griffin, J. A. Zimmerman, and J. D. Hinnefeld, Phys. Rev. C **58**, 3442 (1998).
[31] J. J. Kolata, V. Guimarães, D. Peterson, P. Santi, R. White-Stevens, P. A. DeYoung, G. F. Peaslee, B. Hughey, B. Atalla, M. Kern, P. L. Jolivette, J. A. Zimmerman, M. Y. Lee, F. D. Becchetti, E. F. Aguilera, E. Martinez-Quiroz, and J. D. Hinnefeld, Phys. Rev. Lett. **81**, 4580 (1998).
[32] C. Signorini, Z. H. Liu, A. Yoshida, T. Fukuda, Z. C. Li, K. E. G. Lōbner, L. Müller, Y. H. Pu, K. Rudolph, F. Soramel, C. Zotti, and J. L. Sida, Eur. Phys. J. A **2**, 227 (1998).
[33] E. F. Aguilera, J. J. Kolata, F. M. Nunes, F. D. Becchetti, P. A. De Young, M. Goupell, V. Guimarães, B. Hughey, M. Y. Lee, D. Lizcano, E. Martinez-Quiroz, A. Nowlin, T. W. O'Donnell, G. F. Peaslee, D. Peterson, P. Santi, and R. White-Stevens, Phys. Rev. Lett. **84**, 5058 (2000).
[34] M. Trotta, J. L. Sida, N. Alamanos, A. Andreyev, F. Auger, D. L. Balabanski, C. Borcea, N. Coulier, A. Drouart, D. J. C. Durand, G. Georgiev, A. Gillibert, J. D. Hinnefeld, M. Huyse, C. Jouanne, V. Lapoux, A. Lépine, A. Lumbroso, F. Marie, A. Musumarra, G. Neyens, S. Ottini, R. Raabe, S. Ternier, P. Van Duppen, K. Vyvey, C. Volant, and R. Wolski, Phys. Rev. Lett. **84**, 2342 (2000).
[35] E. F. Aguilera, J. J. Kolata, F. D. Becchetti, P. A. De Young, J. D. Hinnefeld, Á. Horváth, L. O. Lamm, Hye-Young Lee, D. Lizcano, E. Martinez-Quiroz, P. Mohr, T. W. O'Donnell, D. A. Roberts, and G. Rogachev, Phys. Rev. C **63**, 061603(R) (2001).
[36] J. L. Sida, N. Alamanos, C. Daniel, V. Lapoux, M. Trotta, A. Andreyev, F. Auger, D. L. Balabanski, C. Borcea, N. Coulier,

A. Drouart, D. J. C. Durand, G. Georgiev, A. Gillibert, J. D. Hinnefeld, M. Huyse, C. Jouanne, A. Lépine, A. Lumbroso, F. Marie, A. Musumarra, G. Neyens, S. Ottini, R. Raabe, S. Ternier, P. Van Duppen, K. Vyvey, C. Volant, and R. Wolski, Nucl. Phys. **A685**, 51c (2001).

[37] A. Di Pietro, P. Figuera, F. Amorini, C. Angulo, G. Cardella, S. Cherubini, T. Davinson, D. Leanza, J. Lu, H. Mahmud, M. Milin, A. Musumarra, A. Ninane, M. Papa, M. G. Pellegriti, R. Raabe, F. Rizzo, C. Ruiz, A. C. Shotter, N. Soic, S. Tudisco, and L. Weissman, Phys. Rev. C **69**, 044613 (2004).

[38] R. Raabe, J. L. Sida, J. L. Charvet, N. Alamanos, C. Angulo, J. M. Casandjian, S. Courtin, A. Drouart, D. J. C. Durand, P. Figuera, A. Gillibert, S. Heinrich, C. Jouanne, V. Lapoux, A. Lépine-Szily, A. Musumarra, L. Nalpas, D. Pierroutsakou, M. Romoli, K. Rusek, and M. Trotta, Nature (London) **431**, 823 (2004).

[39] L. R. Gasques, L. C. Chamon, D. Pereira, M. A. G. Alvarez, E. S. Rossi Jr., C. P. Silva, and B. V. Carlson, Phys. Rev. C **69**, 034603 (2004).

[40] L. C. Chamon, L. R. Gasques, D. Pereira, and B. V. Carlson, Prog. Theor. Phys. Suppl. **154**, 169 (2004).

[41] L. C. Chamon, B. V. Carlson, L. R. Gasques, D. Pereira, C. De Conti, M. A. G. Alvarez, M. S. Hussein, M. A. Cândido Ribeiro, E. S. Rossi Jr., and C. P. Silva, Phys. Rev. C **66**, 014610 (2002).

[42] I. J. Thompson, Comput. Phys. Rep. **7**, 167 (1988).

[43] H. Feldmeier and J. Schnack, Rev. Mod. Phys. **72**, 655 (2000).

[44] D. M. Brink, in *Proceedings of the International School of Physics, 'Enrico Fermi' Course 36* (Academic Press, New York/London, 1966), p. 247.

[45] H. Horiuchi and K. Ikeda, *Cluster Models and Other Topics* (World Scientific, Singapore, 1986).

[46] R. Roth, T. Neff, H. Hergert, and H. Feldmeier, Nucl. Phys. **A745**, 3 (2004).

[47] H. Friedrich, Phys. Rep. **74**, 209 (1981).

[48] G. Rawitscher, Nucl. Phys. **85**, 337 (1966).

[49] P. Christensen and Z. Switkoswki, Nucl. Phys. **A280**, 205 (1977).

[50] M. A. Cândido Ribeiro, L. C. Chamon, D. Pereira, M. S. Hussein, and D. Galetti, Phys. Rev. Lett. **78**, 3270 (1997).

[51] L. C. Chamon, D. Pereira, M. S. Hussein, M. A. Cândido Ribeiro, and D. Galetti, Phys. Rev. Lett. **79**, 5218 (1997).

[52] L. C. Chamon, D. Pereira, and M. S. Hussein, Phys. Rev. C **58**, 576 (1998).

[53] M. A. G. Alvarez, L. C. Chamon, M. S. Hussein, D. Pereira, L. R. Gasques, E. S. Rossi Jr., and C. P. Silva, Nucl. Phys. **A723**, 93 (2003).

[54] M. A. Alvarez, L. C. Chamon, D. Pereira, E. S. Rossi Jr., C. P. Silva, L. R. Gasques, H. Dias, and M. O. Roos, Nucl. Phys. **A656**, 187 (1999).

[55] C. P. Silva, M. A. G. Alvarez, L. C. Chamon, D. Pereira, M. N. Rao, E. S. Rossi Jr., L. R. Gasques, M. A. E. Santo, R. M. Anjos, J. Lubian, P. R. S. Gomes, C. Muri, B. V. Carlson, S. Kailas, A. Chatterjee, P. Singh, A. Shrivastava, K. Mahata, and S. Santra, Nucl. Phys. **A679**, 287 (2001).

[56] L. R. Gasques, L. C. Chamon, C. P. Silva, D. Pereira, M. A. G. Alvarez, E. S. Rossi Jr., V. P. Likhachev, B. V. Carlson, and C. De Conti, Phys. Rev. C **65**, 044314 (2002).

[57] E. S. Rossi Jr., D. Pereira, L. C. Chamon, C. P. Silva, M. A. G. Alvarez, L. R. Gasques, J. Lubian, B. V. Carlson, and C. De Conti, Nucl. Phys. **A707**, 325 (2002).

[58] L. R. Gasques, L. C. Chamon, D. Pereira, V. Guimarães, A. Lépine-Szily, M. A. G. Alvarez, E. S. Rossi Jr., C. P. Silva, B. V. Carlson, J. J. Kolata, L. Lamm, D. Peterson, P. Santi, S. Vincent, P. A. De Young, and G. Peasley, Phys. Rev. C **67**, 024602 (2003).

[59] L. R. Gasques, L. C. Chamon, D. Pereira, M. A. G. Alvarez, E. S. Rossi Jr., C. P. Silva, G. P. A. Nobre, and B. V. Carlson, Phys. Rev. C **67**, 067603 (2003).

[60] G. R. Satchler and W. G. Love, Phys. Rep. **55**, 183 (1979).

[61] S. Raman, C. W. Nestor, Jr., and P. Tikkanen, At. Data Nucl. Data Tables **78**, 1 (2001).

[62] T. Kibédi and R. H. Spear, At. Data Nucl. Data Tables **80**, 35 (2002).

[63] P. Ring and P. Schuck, *The Nuclear Many-Body Problem* (Springer-Verlag, Berlin, Heidelberg, 2000).

[64] J. F. Berger, M. Girod, and D. Gogny, Comput. Phys. Commun. **63**, 365 (1991).

[65] B. D. Serot and J. D. Walecka, Int. J. Mod. Phys. E **6**, 515 (1997).

[66] D. Vretenar, A. V. Afanasjev, G. A. Lalazissis, and P. Ring, Phys. Rep. **409**, 101 (2005).

[67] T. Gonzalez-Llarena, J. L. Egido, G. A. Lalazissis, and P. Ring, Phys. Lett. **B379**, 13 (1996).

[68] A. V. Afanasjev, P. Ring, and J. König, Nucl. Phys. **A676**, 196 (2000).

[69] G. A. Lalazissis, J. König, and P. Ring, Phys. Rev. C **55**, 540 (1997).

[70] G. A. Lalazissis, T. Niksic, D. Vretenar, and P. Ring, Phys. Rev. C **71**, 024312 (2005).

[71] A. V. Afanasjev, J. König, and P. Ring, Phys. Rev. C **60**, 051303(R) (1999).

[72] A. V. Afanasjev, T. L. Khoo, S. Frauendorf, G. A. Lalazissis, and I. Ahmad, Phys. Rev. C **67**, 024309 (2003).

[73] G. A. Lalazissis, D. Vretenar, and P. Ring, Phys. Rev. C **57**, 2294 (1998).

[74] G. Hulke, C. Rolfs, and H. P. Trautvetter, Z. Phys. A **297**, 161 (1980).

[75] A. Kuronen, J. Keinonen, and P. Tikkanen, Phys. Rev. C **35**, 591 (1987).

[76] S.-C. Wu and C. A. Barnes, Nucl. Phys. **A422**, 373 (1984).

[77] D. G. Kovar, D. F. Geesaman, T. H. Braid, Y. Eisen, W. Henning, T. R. Ophel, M. Paul, K. E. Rehm, S. J. Sanders, P. Sperr, J. P. Schiffer, S. L. Tabor, S. Vigdor, B. Zeidman, and F. W. Prosser, Phys. Rev. C **20**, 1305 (1979).

[78] J. Thomas, Y. T. Chen, S. Hinds, K. Langanke, D. Meredith, M. Olson, and C. A. Barnes, Phys. Rev. C **31**, 1980 (1985).

[79] T. Neff, H. Feldmeier, and K. Langanke, arXiv:nucl-th/0703030.

[80] T. Neff and H. Feldmeier, Nucl. Phys. **A713**, 311 (2003).

[81] R. Roth, H. Hergert, P. Papakonstantinou, T. Neff, and H. Feldmeier, Phys. Rev. C **72**, 034002 (2005).

[82] D. Baye, P.-H. Heene, and M. Libert-Heinemann, Nucl. Phys. **A291**, 230 (1977).

[83] C. L. Jiang, K. E. Rehm, B. B. Back, and R. V. F. Janssens, Phys. Rev. C **75**, 015803 (2007).